

MEASUREMENTS OF HIGH DENSITY MATTER AT RHIC

Peter Jacobs*

Lawrence Berkeley National Laboratory,
Berkeley, CA 94720

ABSTRACT

QCD predicts a phase transition between hadronic matter and a Quark Gluon Plasma at high energy density. The Relativistic Heavy Ion Collider (RHIC) at Brookhaven National Laboratory is a new facility dedicated to the experimental study of matter under extreme conditions. I will discuss the first round of experimental results from colliding heavy nuclei at RHIC and our current understanding of the state of matter generated in such collisions, concentrating on partonic energy loss and jet quenching as a probe of the medium.

*pmjacobs@lbl.gov

1 Introduction

At high temperature or baryon density, hadronic matter dissolves into a soup of its constituent quarks and gluons. For an asymptotically free field theory such as QCD, the state of matter at high energy density is simple¹: long range (low momentum) interactions are screened, and short range (high momentum) interactions are weak, leading to an ideal gas equation of state in the high energy density limit. At temperature $T \gg \Lambda_{\text{QCD}}$ matter is a gas of deconfined, weakly interacting quarks and gluons (the “Quark-Gluon Plasma”, or QGP), whereas at $T \ll \Lambda_{\text{QCD}}$ quarks and gluons are confined and matter consists of strongly interacting hadrons.

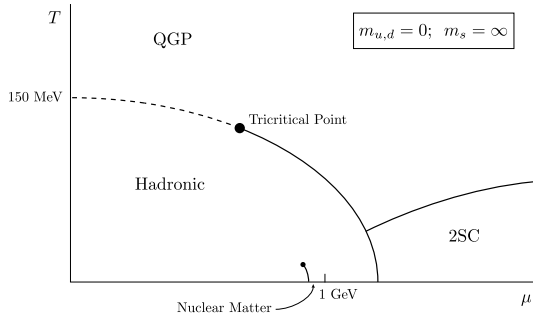


Fig. 1. Example of the QCD phase diagram (temperature T vs. baryochemical potential μ_B) for two massless flavors.² Chiral symmetry is broken in the hadronic phase. “2SC” is a color-superconducting phase.

The QCD phase diagram has a complex structure (Fig. 1). At low temperature and baryon density the phase is hadronic (confined phase) and chiral symmetry is broken. Color-superconducting and other phases may exist at high baryon density and low temperature,² whereas at high temperature the quarks and gluons are deconfined and chiral symmetry is restored. The early universe descended from high T at extremely small μ_B . Neutron star cores have high μ_B and very low T .

First-principles calculations of finite temperature QCD can only be carried out numerically on the lattice.³ Fig. 2 shows a recent lattice calculation of the energy density ϵ as function of temperature for two- and three-flavor QCD. ϵ exhibits a sharp rise in the vicinity of the critical temperature T_C , indicating a rapid change in the density of underlying degrees of freedom. The ideal gas Stefan-Boltzmann limit ϵ_{SB} has not yet been achieved at $T \sim 4T_C$. Putting in physical values, $T_C \sim 175 \text{ MeV}$, resulting in critical energy density $\epsilon_C = (6 \pm 2)T_C^4 \sim 1 \text{ GeV}/\text{fm}^3$. This value should be kept in mind for comparison to conditions achieved in laboratory experiments.

The order of the deconfinement phase transition can be determined in some limiting cases.³ It is first order for pure gauge and for three light quarks, second order for two light and one heavy quark. For physical quark masses the order of the transition, or

indeed whether it is a smooth cross over, has not been determined. The extension of lattice calculations to $\mu_B \neq 0$ is a long-standing problem, but there has been significant recent progress in determining the phase boundary and equation of state for finite μ_B .⁵

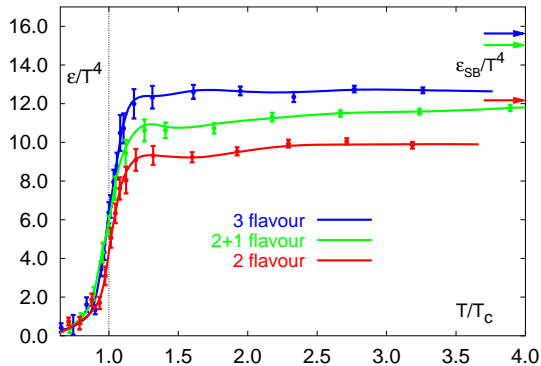


Fig. 2. Lattice calculation of energy density vs temperature for two- and three-flavor QCD.⁴

It is natural to ask whether the deconfinement and chiral symmetry restoration transitions can be studied in accelerator-based experiments. We require a system having temperature of order the pion mass in equilibrium over a large volume. The best possibility to accomplish this is through the collision of heavy nuclei at the highest possible energy.

However, nuclear collisions at high energy are highly dynamic. Even if a hot, equilibrated system is created early in the collision, it will immediately expand and cool. If a QGP is formed it will hadronize after a brief period, and signatures from the deconfined phase may be masked by those from the hot, interacting hadron gas. The central issue is to find and measure those experimental observables that are sensitive to the state of matter early in the collision.⁸

Broadly speaking, several epochs in the evolution of high energy nuclear collisions can be sketched. Immediately following the collision is a brief formation time $\tau < 1$ fm/c, during which large momentum transfer (short-distance) processes occur. It is also during this period that the highest energy density is achieved and the QGP may result. After an expansion time of perhaps a few fm/c the plasma hadronizes into a dense, interacting hadron gas. Further expansion and cooling causes the temperature to fall to the point at which inelastic collisions among hadrons are no longer common (*chemical freezeout*) and the relative populations of the various long-lived hadron species are es-

In the early universe, the confinement transition (QGP \rightarrow hadrons) at very low μ_B occurred about 10 microseconds after the big bang.⁶ A strongly first order phase transition may have generated primordial black holes, strange quark nuggets, or local baryon asymmetries affecting primordial nucleosynthesis, though no relics of this transition have been observed thus far. In the cores of neutron stars, a QGP phase at low temperature and high μ_B may generate observable millisecond pulsar phenomena.⁷

established. Elastic collisions occur until *kinetic freezeout*, after which point the hadrons fly effectively undisturbed to the detectors. Thus, the relative populations of stable hadrons reflect the conditions at chemical freezeout, whereas their momentum spectra reflect the conditions at kinetic freezeout. More penetrating probes (dileptons, direct photons, jets, heavy quarks,...) may carry information on the conditions around the time of their formation earlier in the collision.

Collisions of heavy nuclei at ultra-relativistic energies have been studied in fixed target experiments at the Brookhaven AGS and CERN SPS for the past 15 years. In 1999, the Relativistic Heavy Ion Collider (RHIC) at Brookhaven National Laboratory was commissioned, bringing into operation the first facility largely dedicated to the study of matter at high energy density.

I will first describe the RHIC machine and experiments and then discuss some of the main results from its heavy ion physics program. I will briefly touch on “soft physics” observables ($p_T < \sim 2 \text{ GeV}/c$) and summarize what has been learned from them. The bulk of the review concentrates on the major new development at RHIC: jet production and indications of partonic interactions with dense matter, which may directly probe the energy density achieved early in the collision.

2 The Relativistic Heavy Ion Collider

RHIC consists of two independent superconducting rings, 3.8 km in length. It has enormous flexibility in beam masses and energies, with capability to collide gold ions from $\sqrt{s_{NN}}=20$ to 200 GeV per nucleon pair, protons up to $\sqrt{s}=500$ GeV, and asymmetric systems, most importantly protons and deuterons with heavy nuclei. The top CM energy for heavy nuclei is a factor 10 larger than for the fixed target experiments, extending significantly the statistical and transverse momentum reach of many observables and opening up new channels. RHIC is also the first polarized proton collider, opening new opportunities to study the spin content of the proton, in particular the contribution of the gluon at low x_{Bj} . More details of the machine and its first year performance can be found in Ref. (9).

Design luminosity for Au+Au at 200 GeV is $\mathcal{L} = 2 \cdot 10^{26} \text{ cm}^{-2}\text{sec}^{-1}$, giving an interaction rate of about 2 kHz. While this luminosity appears to be tiny relative to other modern colliders, recall that the rate for hard processes such as jet production in nuclear collisions scales as $\sim A^2$ (A =atomic mass), so that hard process rates in Au+Au at design luminosity are the same as at a proton collider with $\mathcal{L} \approx 10^{31} \text{ cm}^{-2}\text{sec}^{-1}$.

The design luminosity for p+p collisions at 500 GeV is $2 \cdot 10^{32} \text{ cm}^{-2}\text{sec}^{-1}$, with an interaction rate of about 8 MHz. Design polarization for p+p is 70%.

RHIC has six intersection regions, of which four are currently instrumented with experiments.¹⁰ PHENIX consists of an axial field magnet and four independent spectrometers: two at midrapidity containing tracking, ring imaging Cerenkov counters, time of flight, and electromagnetic calorimetry, which are optimized for precision lepton, photon and hadron measurements, and two forward muon arms. STAR has conventional collider detector geometry, with a large solenoidal magnet, Time Projection Chamber for tracking, large coverage EM calorimetry, and an inner silicon-based tracker. STAR is designed for hadron, jet, lepton and photon measurements over large acceptance, as well as studies of event-wise fluctuations in high multiplicity nuclear collisions. BRAHMS consists of two small acceptance spectrometers for inclusive identified hadron measurements over wide phase space. PHOBOS has very wide phase space coverage for charged particles using silicon detectors, and a mid-rapidity spectrometer based on a dipole magnet, silicon tracking and Time of Flight. STAR and PHENIX each have about 450 collaborators, whereas PHOBOS and BRAHMS each have fewer than 100.

RHIC had a brief commissioning run in 1999. The data reported here are from a Au+Au run at $\sqrt{s_{NN}}=130$ GeV in 2000 and Au+Au and polarized p+p ($\sim 15\%$ polarization) runs at $\sqrt{s_{NN}}=200$ GeV in 2001-2. The integrated luminosity is about $80 \mu\text{b}^{-1}$ for Au+Au and 1 pb^{-1} for p+p. A comprehensive view of the physics program of RHIC and what has been achieved thus far can be found in the proceedings of the recent Quark Matter conferences.^{11,12}

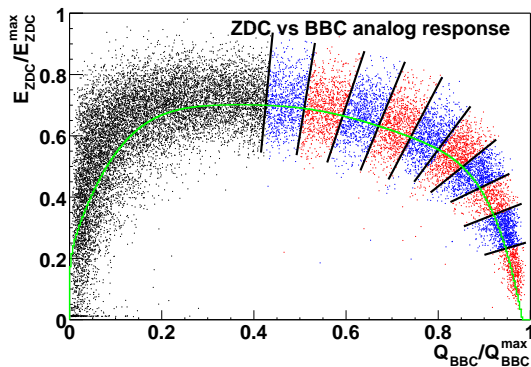


Fig. 3. Event characterization¹⁴: correlation of ZDC signal (vertical) with multiplicity.

Nuclei are extended objects, and high energy nuclear collisions can be characterized experimentally as head-on (“central”) or glancing (“peripheral”). For this purpose all experiments have identical forward hadron calorimeters (Zero Degree Calorimeters, or ZDCs¹³), situated ± 18 m downstream of the interaction region beyond the first machine dipole magnets. The ZDCs measure the forward-going “spectator” neutrons which did not scatter significantly. The

correlation of the ZDC signal with the event multiplicity serves to characterize the geometry of the event. Peripheral collisions have few spectator neutrons and low multiplicity. More central collisions generate more spectator neutrons and higher multiplicity, while the most central, head-on collisions again generate few spectator neutrons and the highest multiplicity. Fig. 3 shows this correlation from the PHENIX experiment, the other experiments use similar distributions. Based on this correlation the total geometric cross section can be divided into bins containing a certain percentile of “centrality”, as shown by the lines on the figure.

Related quantities which also characterize the centrality of the event are the number of incoming participating nucleons (N_{part}), and the number of equivalent binary nucleon-nucleon collisions (N_{binary}). N_{part} and N_{binary} are calculated for each centrality bin using the Glauber formalism and a realistic model of the nuclear geometry.¹⁵ Phenomenologically it has been found that total particle production scales roughly as N_{part} , whereas the rate of hard processes will scale as N_{binary} in the absence of nuclear effects. Such scaling rules can be used to uncover the new physics present in nuclear collisions. For instance, the violation of N_{binary} scaling at high p_T indicates significant effects of the nuclear medium on high p_T processes. I will return to this point below.

3 Soft Physics

Fig. 4 from the PHOBOS Collaboration¹⁶ shows charged particle multiplicity distributions $dN_{ch}/d\eta$ vs η ¹⁷ over the full RHIC phase space, for Au+Au collisions at all three collision energies studied so far. The longitudinal phase space growth with increasing energy is apparent, as well as the increase in multiplicity for more central collisions. For the most central collisions at $\sqrt{s_{NN}}=130$ GeV, 4200 charged particles are produced in the full phase space.

Figure 4 exhibits a central plateau near $\eta \sim 0$, indicating that the system has approximate longitudinal boost invariance. More detailed considerations of identified particle spectra show that boost invariance holds over a rather smaller region $\Delta y \sim 1$.¹⁸ Bjorken studied boost invariant hydrodynamics¹⁹ and derived a useful pocket formula for the energy density achieved in the central region:

$$\epsilon_{\text{Bj}} = \frac{1}{\pi R_A^2 \tau} \frac{dE_T}{dy} \approx \frac{1}{\pi R_A^2 \tau} \langle p_T \rangle \frac{3}{2} \frac{dN_{ch}}{d\eta}, \quad (1)$$

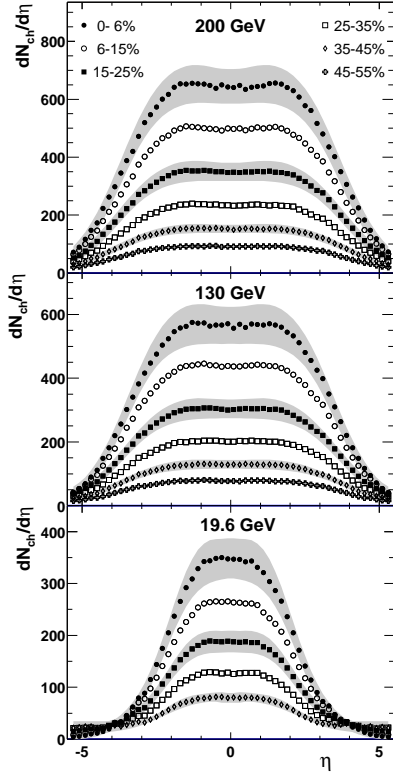


Fig. 4. $dN_{ch}/d\eta$ for various collision centralities over the full RHIC phase space.¹⁶

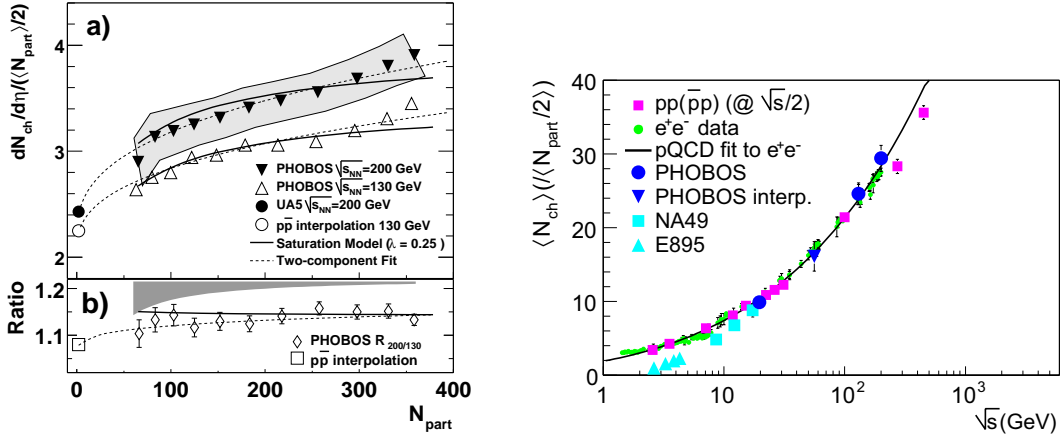
where E_T and $dN_{ch}/d\eta$ are the transverse energy and multiplicity density (Fig. 4). R_A is the nuclear radius and τ is the formation time, typically taken as ~ 1 fm/c, after which the hydrodynamic description is valid. PHENIX measured E_T for central Au+Au collisions at $\sqrt{s_{NN}}=130$ GeV and derived an energy density of 4.6 GeV/fm³,²⁰ well above 1 GeV/fm³ required for the deconfinement transition as calculated on the lattice. Conditions appear to be favorable to form a QGP in nuclear collisions at RHIC, though under the assumption that an equilibrated system is established after a time ~ 1 fm/c.

Scaling of global observables such as multiplicity with collision centrality and \sqrt{s} has been discussed extensively in the context of gluon saturation (e.g. Ref. 15 and references therein). A projectile parton at sufficiently low x interacts coherently with all partons in the target that lie within a transverse area $1/Q^2$, with cross section $\sigma \sim \alpha_s/Q^2$. If the target is a heavy nucleus, its finite thickness will increase the parton density seen by the probe: nuclei are “blacker” than protons. The Q^2 scale at which the nucleus becomes dense to the probe is given by the saturation condition¹⁵:

$$Q_s^2 \sim \alpha_s(Q_s^2) \frac{xG_A(x, Q_s^2)}{\pi R_A^2} \sim A^{\frac{1}{3}}, \quad (2)$$

where $xG_A \sim A$ is the nuclear gluon distribution and $R_A \sim A^{\frac{1}{3}}$ is the nuclear radius. For central Au+Au collisions at RHIC $Q_s^2 \sim 2$ GeV², so that $\alpha_s(Q_s^2)$ is small: in the saturation regime the coupling is weak while the gluon density is high, leading to classical, nonlinear dynamics. The growth of Q_s^2 with target thickness leads e.g. to definite predictions for the dependence of multiplicity on collision centrality.¹⁵

Fig. 5(a) from PHOBOS illustrates this dependence for Au+Au collisions at 130 and 200 GeV (central collisions correspond to large number of participants N_{part} , peripheral to small N_{part}). The data are compared to both the saturation model and a more conventional “two component” model, which parameterizes the centrality dependence



(a) Multiplicity ($\eta \sim 0$) per participant pair vs. centrality.²¹

(b) Universal scaling of total multiplicity vs. \sqrt{s} for e^+e^- , p+p and Au+Au.²²

Fig. 5.

of multiplicity in terms of soft production (scaling with N_{part}) and minijet production (scaling with N_{binary}). The data are consistent with both models and cannot resolve the small difference between them. While this is a very active area of research, no clear evidence of saturation effects in nuclear collisions has been found yet at RHIC.

Fig. 5(b) from PHOBOS shows a universal scaling of the total multiplicity with \sqrt{s} for e^+e^- , p+p and Au+Au.²² (The p+p data are corrected for energy carried by the leading particles.) This is at first sight surprising, given the very different nature of the various systems, but may point to universal features of particle production in high energy collisions (though it should also be noted that the evolution with \sqrt{s} of the mean transverse momentum shows no such scaling among the various systems¹⁸).

As argued above, the relative population of the stable hadrons is fixed at chemical freezeout. Equilibrium at that point should be evident in the measured population ratios. Fig. 6 shows population ratios measured at mid-rapidity for a wide variety of non-strange and strange hadrons, with values varying over three orders of magnitude. Also shown are results from a statistical model fit to the data.²³ The model consists of a partition function containing contributions from all baryons and mesons with mass less than 2 GeV, with two free parameters (chemical freezeout temperature T_{chem} and baryochemical potential μ_B) and constraints due to strangeness and charge conservation. The resulting fit from this and similar models is excellent, with extracted parameters $T_{chem} \sim 170$ MeV and $\mu_B \sim 25 - 50$ MeV, close to the critical temperature for the

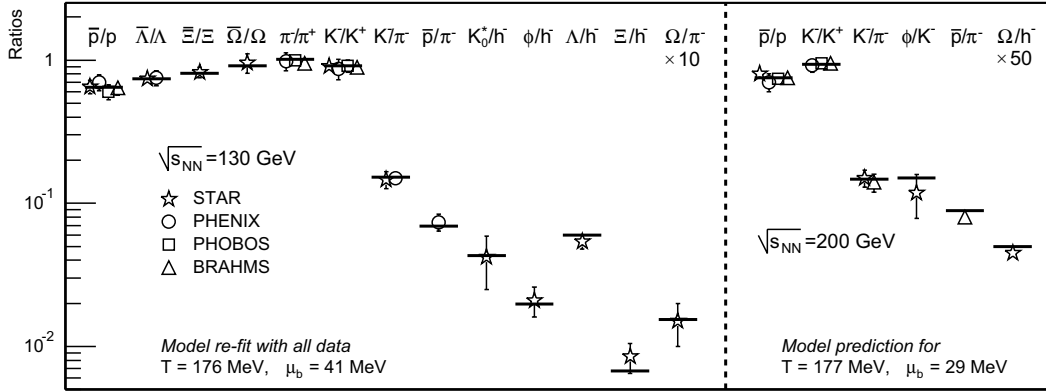


Fig. 6. Population ratios of stable hadrons and statistical model fit.^{23,18}

deconfinement phase transition calculated on the lattice. A hadronic gas cannot exist at a higher temperature, suggesting that equilibrium is in fact established *prior* to hadronization, in the deconfined phase.

I cannot hope to address all the soft physics observables that have been studied at RHIC. To conclude this section I will summarize a few of the main results, more detailed discussions can be found in Refs. (12,18).

- Low baryon density: antibaryon/baryon ratios at midrapidity are $\sim 0.6-1.0$. The system is close to baryon free, similar to the early universe, but not precisely so. Finite baryon number is transported $\Delta y \sim 5.5$ rapidity units from the beam.
- There are strong indications that hadronic chemical equilibrium has been achieved at a temperature near the lattice critical temperature.
- Hydrodynamic calculations describe well the transverse momentum spectra and “elliptic flow” (see below). The mass dependence of these observables, which is a sensitive test of the hydrodynamic picture, is described in detail.
- The energy density achieved early in the collision is estimated to be $\sim 5 \text{ GeV}/\text{fm}^3$.
- Identical two-particle correlations (Hanbury Brown-Twiss correlations) are sensitive to the space-time evolution of the source. The extracted source radii and duration of freezeout show no significant increase relative to lower energy nuclear collisions. Such correlations measure only a piece of a dynamically expanding source and these results may indicate a very explosive expansion resulting from high early pressure.

4 High p_T Hadrons and Jets

The increase in $\sqrt{s_{NN}}$ for nuclear collisions at RHIC relative to fixed target experiments opens up new channels to probe the dense medium generated in the collision. Jets with $E_T \sim 40$ GeV and higher are produced in sufficient numbers to provide robust observables. The measurement of jets in nuclear collisions poses a special problem, however: while the presence of a hard scattering in a nuclear collision can be detected (though in a biased way) via high p_T leading hadrons, the huge soft multiplicities seen in Fig. 4 contaminate any finite jet cone, spoiling the jet energy measurement. At sufficiently high E_T this effect may be minor (e.g. nuclear collisions at the LHC), but for the jet E_T currently accessible at RHIC it is fatal. We therefore restrict our considerations to leading particles and their correlations. We show below that hadrons with $p_T > \sim 4$ GeV/c are produced dominantly from jet fragmentation, even in the most central Au+Au collisions.

Twenty years ago Bjorken²⁴ proposed that hard scattered partons in nuclear collisions could provide a sensitive probe of the surrounding medium. The energy loss dE/dx due to elastic scattering of the partons in a Quark Gluon Plasma depends on the temperature as T_{plasma}^2 and results in a suppression of the observed rate of jets or their leading hadrons at fixed p_T . Later work showed that dE/dx from elastic scattering is negligible but that radiative energy loss in dense matter could be considerable.^{25,26,27} The energy loss is directly sensitive to the gluon density of the medium, ρ_{glue} . While not a direct signature of deconfinement, measurement of ρ_{glue} that is substantially larger than in cold nuclear matter²⁸ is incompatible with the presence of a hadronic medium, thus large energy loss serves as an indirect signature of deconfinement.

There are currently three sets of measurements which address the question of partonic energy loss in dense matter, which I will discuss in turn: suppression of inclusive spectra, elliptic flow (azimuthal asymmetry) in non-central events, and correlations of high p_T hadron pairs.

4.1 High p_T : Suppression of Inclusive Spectra

In p+p collisions at RHIC energies, hadrons with $p_T \sim 4$ GeV/c typically carry 75% of the energy of their parent jet, leading to the possibility that partonic energy loss in Au+Au collisions is reflected in the suppression of leading hadrons.²⁷ Hadron suppression is measured via the nuclear modification factor:

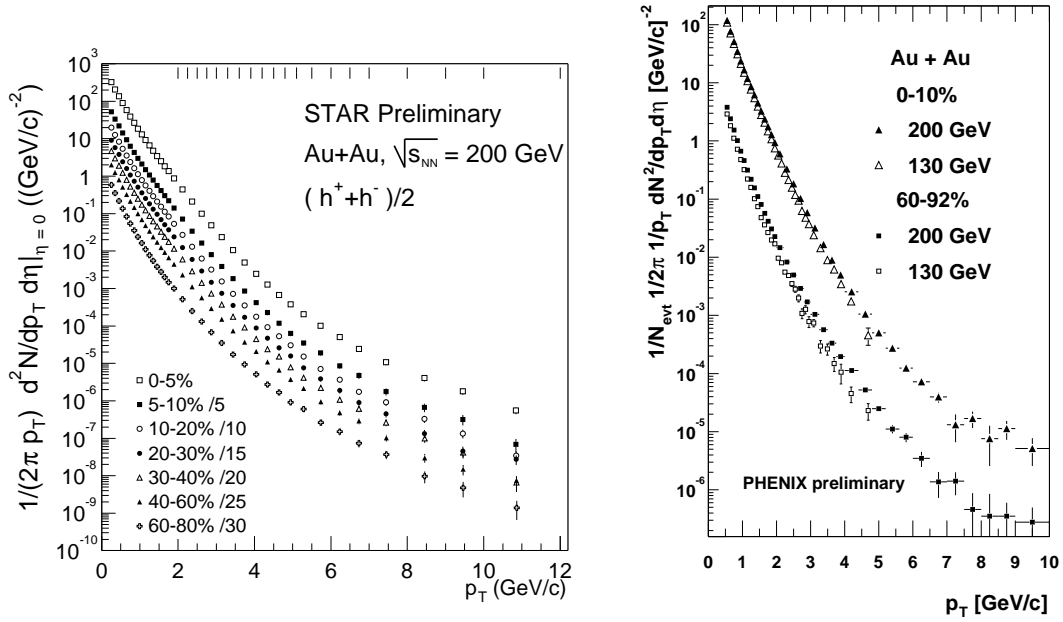


Fig. 7. Inclusive charged hadron invariant distributions for various event centralities.²⁹

$$R_{AA}(p_T) = \frac{d\sigma_{AA}/dydp_T^2}{\langle N_{\text{binary}} \rangle d\sigma_{pp}/dydp_T^2} \quad (3)$$

where $\sigma_{pp}/dydp_T$ is the inclusive cross section measured in elementary nucleon-nucleon collisions and $\langle N_{\text{binary}} \rangle$ accounts for the geometric scaling from the elementary to nuclear collision. $R_{AA}(p_T)$ is normalized to be unity if Au+Au collisions are an incoherent superposition of p+p collisions. In addition to partonic energy loss, $R_{AA}(p_T)$ may be altered by nuclear effects such as gluon shadowing, which will reduce $R_{AA}(p_T)$, and the Cronin effect (multiple soft scattering in the initial state), which will increase it. These effects must be disentangled using measurements in simpler systems (in particular p+Au).

First indication of a strong suppression of high p_T hadrons in nuclear collisions was reported from the 130 GeV data by both PHENIX and STAR.²⁹ The 200 GeV data have much higher statistics and both collaborations have now pushed this study well into the perturbative regime. Fig. 7 shows the inclusive charged hadron spectra as a function of centrality for Au+Au collisions at 200 GeV, extending to $p_T=12$ GeV. PHENIX has also shown π^0 spectra from both Au+Au and p+p.³⁰ Fig. 8 shows $R_{AA}(p_T)$ for these data. Suppression factors of 4-5 are observed in central collisions for both π^0 s and charged

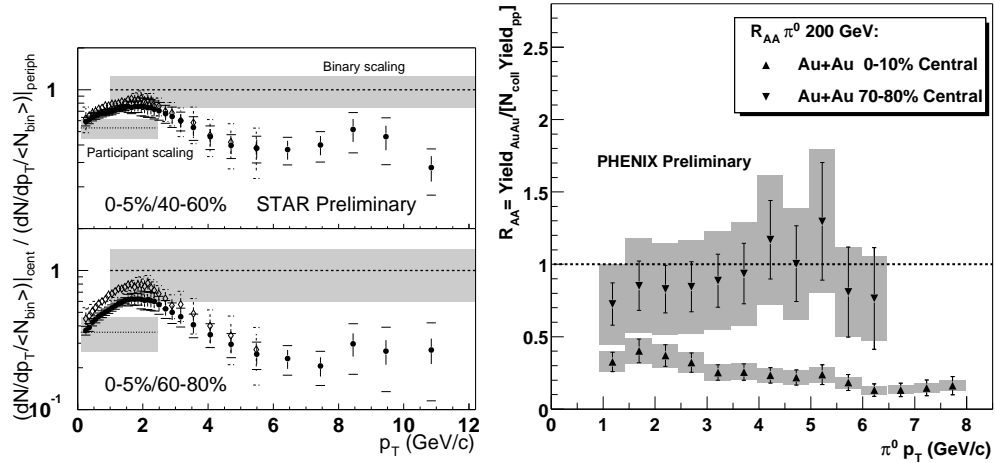


Fig. 8. $R_{AA}(p_T)$ (eq. 3 or slight modification) for charged hadrons (left panel, STAR³¹) and π^0 (right panel, PHENIX³⁰).

hadrons, with weak, if any, dependence on p_T above $p_T \sim 5$ GeV/c. At asymptotically high jet E_T the relative energy loss should be negligible and $R_{AA}(p_T)$ should return to unity. No evidence of this limiting high energy behavior is seen.

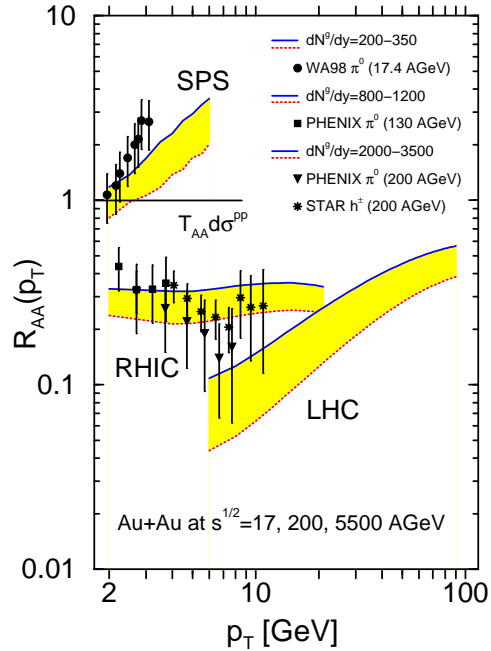


Fig. 9. pQCD calculation of hadron suppression,³² compared to data from Fig. 8.

Fig. 9 shows a pQCD calculation³² incorporating Cronin enhancement, nuclear shadowing and energy loss, compared to the data for central collisions from Fig. 8 as well as lower energy fixed target data. The RHIC data are compatible with a gluon rapidity density $dN^g/dy \sim 800 - 1200$, several times that of cold nuclear matter. The calculation predicts a suppression factor independent of p_T , an effect specific to RHIC energies due to the interplay between the Cronin effect and energy loss. In nuclear collisions at the SPS (fixed target), energy loss is masked by a much larger Cronin effect due to the much more steeply falling inclusive spectrum, while at the LHC partonic energy loss overwhelms other nuclear effects. The clear separation of Cronin

enhancement from energy loss at RHIC awaits the upcoming data from d+Au collisions.

4.2 High p_T : Elliptic Flow

Non-central nuclear collisions generate a transversely asymmetric reaction zone. In high multiplicity events the orientation of the reaction plane can be determined experimentally through measurement of the azimuthal anisotropy of the reaction products.³⁴ The occurrence of an anisotropy in momentum space (“elliptic flow”) is *prima facie* evidence of multiple interactions amongst the reaction products, which convert spatial into momentum-space anisotropy. Furthermore, the asymmetry is generated early in the collision and expansion of the system will only dilute it.³³ The agreement in detail of hydrodynamic calculations with elliptic flow measurements³⁴ for $p_T < 2$ GeV/c (including mass dependence, a sensitive test) argues strongly in favor of local equilibration early in the collision.

Finite azimuthal correlations of high p_T hadrons with the reaction plane can result from partonic interactions in the medium.³⁵ *A priori* the di-jet axis has no correlation with the reaction plane orientation. If the outgoing parton or its hadronic fragments interacts with the surrounding medium, the energy loss will depend upon the length of matter transversed. The consequence will be an azimuthally varying hadron suppression, correlated with the reaction plane.

The strength of this correlation is measured by the elliptic flow coefficient³⁶ $v_2(p_T) = \langle \cos(2\phi) \rangle$, the second coefficient of the Fourier decomposition of the azimuthal distribution relative to the reaction plane. Fig. 10, left panel, shows $v_2(p_T)$ for charged hadrons measured by STAR from minimum bias Au+Au collisions at 130 GeV, together with a calculation patching together hydrodynamics at low p_T and pQCD with partonic energy loss at high p_T .³⁵ The hydrodynamic calculation agrees at $p_T < \sim 2$ GeV/c. There is rough agreement with the pQCD calculation incorporating large initial gluon density at $p_T \sim 4 - 6$ GeV/c. The right panel shows $v_2(p_T)$ for the 200 GeV data, extending the measurement to $p_T \sim 12$ GeV/c. The finite correlation strength persists for all but the most central collisions to $p_T \sim 10$ GeV/c, well into the perturbative regime. Shuryak has pointed out³⁷ that the plateau values of v_2 for $p_T > 2$ GeV/c in Fig. 10 are in fact very large, exhausting (or even exceeding) the asymmetries expected from the initial geometry of the collision.

The reaction plane for the data in Fig. 10 is calculated using hadrons with $p_T < 2$

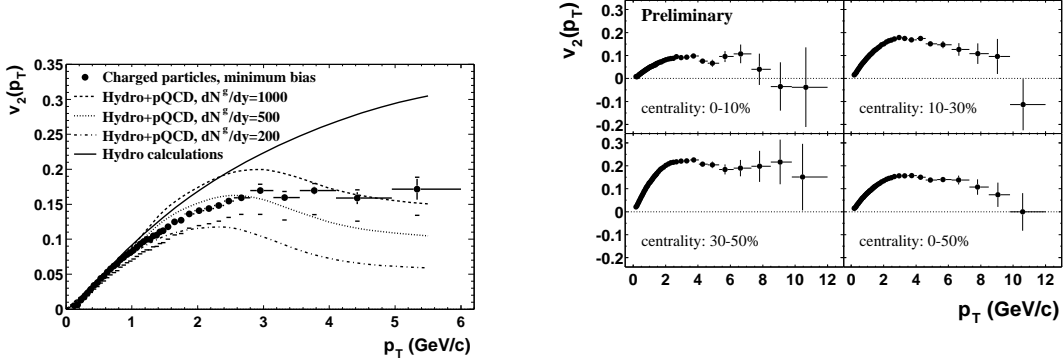
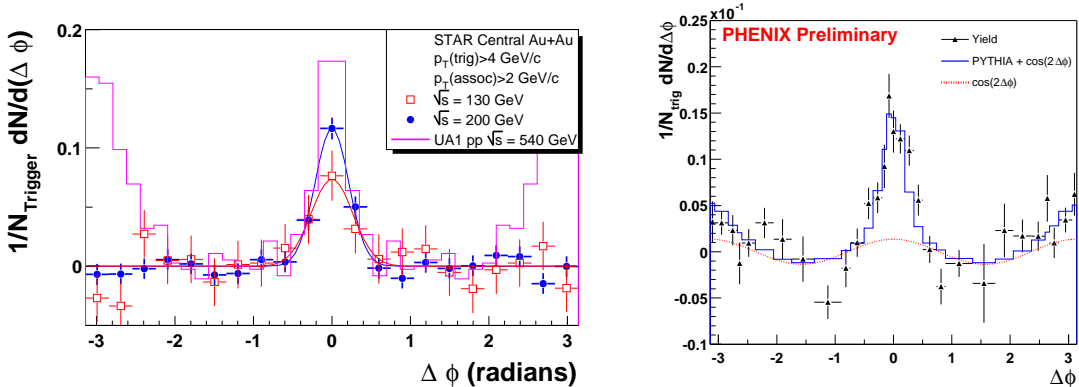


Fig. 10. Elliptic flow $v_2(p_T)$ for charged hadrons. Left panel: minimum bias at 130 GeV compared to pQCD calculation.^{38,35} Right panel: centrality dependence at 200 GeV.³⁹

GeV/c. This measurement may be biased by multiparticle correlations unconnected to the reaction plane (“non-flow” effects), such as resonance decays, momentum conservation or jet fragmentation. At $p_T \sim 4$ GeV/c, non-flow contributes $\sim 20\%$ to $v_2(p_T)$.³⁹ The magnitude of non-flow at higher p_T remains an open problem, though preliminary studies indicate that the non-flow relative contribution does not increase markedly at higher p_T .

4.3 High p_T : Two-particle Correlations

The two previous sections discussed inclusive hadron production and the correlation of single leading hadrons with the reaction plane determined from the bulk of the event ($p_T < 2$ GeV/c). While jet fragmentation is reasonably expected to dominate hadron production at sufficiently high p_T , it remains an open question whether the current measurements have achieved that limit. Full jet reconstruction in Au+Au events is not possible due to the complex underlying event, but intra-jet correlations amongst high p_T hadrons are still visible and we will use these to map the transition in p_T from soft to hard physics. The rate of back-to-back di-jets (di-hadrons) may be especially sensitive to partonic energy loss effects: if one escapes from the surface, its partner has enhanced probability to plow through the bulk matter.



(a) STAR,^{38,40} large $|\Delta\eta|$ subtracted.

(b) PHENIX.³⁰

Fig. 11. Azimuthal distributions of high p_T hadron pairs demonstrating intra-jet correlations. See text for details.

4.3.1 Near-Angle Correlations

We first consider near-angle correlations at high p_T to look for jet-like correlations. In the previous section, however, we showed that high p_T hadrons are azimuthally correlated with the reaction plane (elliptic flow) with strength v_2 , so that even in the absence of jets, high p_T hadron pairs will exhibit a correlation with strength v_2^2 . Elliptic flow and other non-jet contributions must be accounted for to extract quantitatively the correlations due to jets.

Fig. 11 shows the distribution of relative azimuthal angle of high p_T charged hadrons with respect to a trigger:

- Fig. 11(a): the trigger is a charged hadron with $p_T > 4$ GeV/c in the STAR TPC. Correlations due to non-jet effects, in particular elliptic flow, have long range in $\Delta\eta$ (difference in pseudorapidity between the pair), whereas intra-jet correlations have short range in $\Delta\eta$ (caveat: also true of correlations due to resonances). The contribution of non-jet effects to the angular correlation can be assessed by comparing the azimuthal distributions for pairs having $|\Delta\eta| < 0.5$ and $0.5 < |\Delta\eta| < 1.4$. The figure shows the difference between azimuthal distributions for small and large $\Delta\eta$, and the peak at $\Delta\phi = 0$ in the figure is therefore short range in both $\Delta\phi$ and $\Delta\eta$. (The away-side peak due to di-jets is subtracted by construction.) Distributions for Au+Au collisions at 130 and 200 GeV are shown, as well as a similar analysis from UA1 for $\bar{p} + p$ at $\sqrt{s}=540$ GeV (though

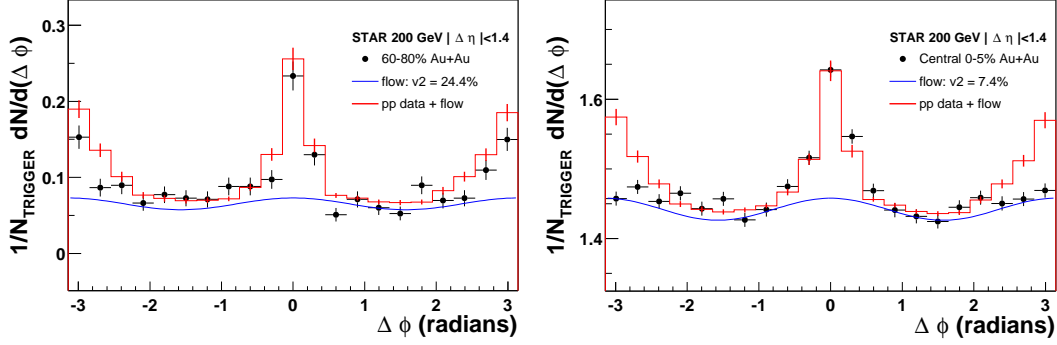


Fig. 12. Azimuthal correlations of high p_T hadron pairs in Au+Au compared to p+p plus elliptic flow (eq. 4).⁴⁰ Left panel: peripheral collisions. Right panel: central collisions.

without the large $|\Delta\eta|$ contribution subtracted). The peak has similar width in all cases and grows in strength with increasing \sqrt{s} , as expected due to the hardening of the underlying jet E_T spectrum with higher \sqrt{s} .

- Fig. 11(b): trigger is a neutral cluster in the PHENIX Electromagnetic Calorimeter with energy > 2.5 GeV, principally photons from high p_T π^0 decays. The azimuthal distribution from the PYTHIA event generator matches correlations from p+p events measured in the same detector, assumed to be due to jets, and PYTHIA is therefore used for comparison to Au+Au. The dashed line shows the expectation from elliptic flow, and the solid line shows the sum of PYTHIA and elliptic flow. The near-angle correlation is clearly dominated by jet contributions.

As an additional check, the near-angle correlation exhibits a preferred charge ordering,⁴⁰ in quantitative agreement with jet fragmentation studies at LEP.⁴¹ The quantitative agreement suggests that hadron production at $p_T > 4$ GeV/c is dominated by jet fragmentation in both p+p and Au+Au.

4.3.2 Back-to-Back Hadron Correlations

We now turn to high p_T hadron pairs with large azimuthal angle difference (back-to-back pairs) and search for the effect of partonic energy loss on the di-jet (di-hadron) production rate.⁴⁰ Fig. 12 shows the azimuthal angular distribution between pairs for the most central and peripheral Au+Au collisions at 200 GeV. The contribution of elliptic flow and other non-jet effects must again be accounted for. Since we are interested

in the correlation strength of back-to-back pairs, which have broad correlation in $\Delta\eta$, the trick used for the near-angle correlations of subtracting the large $\Delta\eta$ distribution will not work. Instead, STAR compares the full azimuthal distribution from p+p and Au+Au events measured in the same detector. The null hypothesis is that high p_T correlations in Au+Au correspond to an *incoherent* superposition of the jet-like correlations measured in p+p and elliptic flow. This is expressed in the following ansatz for the azimuthal distribution in Au+Au:

$$D_2^{\text{AuAu}} = D_2^{\text{pp}} + B(1 + 2v_2^2 \cos(2\Delta\phi)). \quad (4)$$

D_2^{pp} is the azimuthal distribution measured in p+p, v_2 is determined independently (see Fig. 10) and is taken as constant for $p_T > 2$ GeV/c, and B is an arbitrary normalization to account for the combinatorial background, fit in the non-jet region $\Delta\phi \sim \pi/2$.

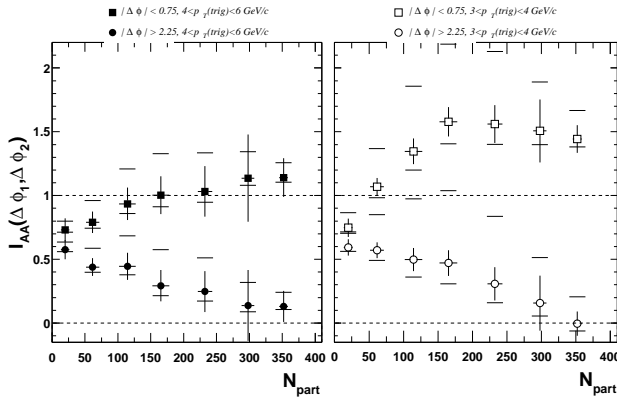


Fig. 13. I_{AA} vs centrality (large N_{part} =central collisions) for near-angle (upper) and back-to-back (lower) angular correlations.⁴⁰ Left: trigger $p_T > 4$ GeV/c. Right: trigger $p_T > 3$ GeV/c.

However, the large angle peak in the most central collisions is not described by eq. 4. We are therefore led to a striking observation: back-to-back jet production is strongly suppressed in the most central Au+Au collisions.

The full centrality dependence of this effect is seen by subtracting the elliptic flow component and normalizing the integrated correlation peaks in Au+Au to those in p+p:

$$I_{AA}(\Delta\phi_1, \Delta\phi_2) = \frac{\int_{\Delta\phi_1}^{\Delta\phi_2} d(\Delta\phi) [D_2^{\text{AuAu}} - B(1 + 2v_2^2 \cos(2\Delta\phi))]}{\int_{\Delta\phi_1}^{\Delta\phi_2} d(\Delta\phi) D_2^{\text{pp}}}. \quad (5)$$

Fig. 13 shows I_{AA} as a function of event centrality for two sets of trigger and as-

The solid lines in fig. 12 show the elliptic flow component and the histograms are the result of eq. 4. At all centralities, the near-angle peak is fit well by eq. 4, as is the large angle peak for peripheral collisions (but slightly less well, see below). Thus, back-to-back hadron pair production in peripheral nuclear collisions is well described by an incoherent superposition of elliptic flow and jet-like correlations measured in p+p. However,

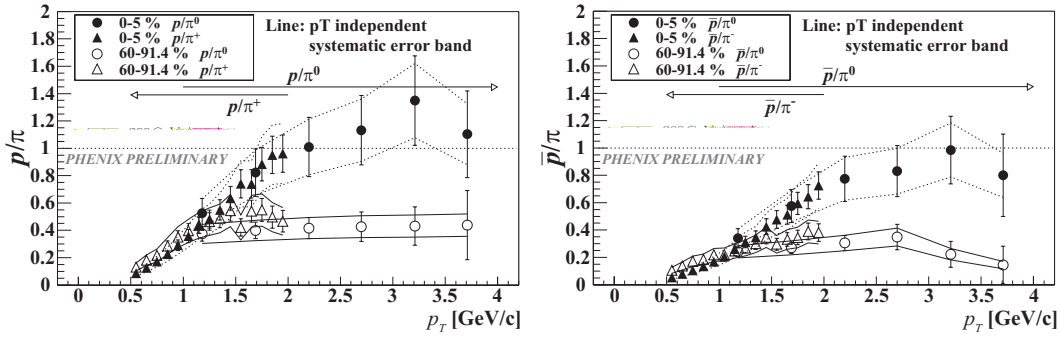


Fig. 14. Ratio of proton to pion yield vs p_T for central (filled) and peripheral (open) collisions.³⁰

sociated particle thresholds. The near-angle peak strength is near or above unity for all centralities and both thresholds: there is no suppression in the near-angle correlation. In contrast, the back-to-back correlation strength in Au+Au relative to p+p decreases smoothly from peripheral to central collisions. For the most central collisions the strength is consistent with zero, which would correspond to a complete suppression of the away-side hadron correlation rate above the threshold.

Various nuclear effects may contribute to the features seen in fig. 13. Initial state multiple scattering might generate both the increase of the near-angle and suppression of the back-to-back correlation strength for more central collisions. The suppression in the most peripheral bin for Au+Au relative to p+p for both the near-angle and back-to-back peaks could be due to nuclear shadowing, or possibly the interplay between multiple scattering and absorption in matter. These issues will be clarified by the upcoming d+Au run at RHIC.

4.4 High p_T : Baryon Enhancement

Near-side azimuthal correlations indicate that hadron production at $p_T > \sim 4$ GeV/c is dominated by jet fragmentation at all centralities. However, Fig. 14 and 15 from the PHENIX Collaboration showing the relative populations of mesons and baryons at high p_T present a challenge to this picture. In fig. 14 the proton/pion ratios for peripheral collisions are in the vicinity of 0.3-0.4, consistent with many measurements of jet fragmentation in elementary collisions, but the ratios for central collisions are near or exceed unity for $p_T \sim 2-4$ GeV/c,³⁰ very unlike conventional jet fragmentation in vacuum. This could be due to transverse radial flow (hydrodynamic behavior), which has

a strong mass dependence,¹⁸ extending “soft” physics into the nominally perturbative regime. A second possibility is the Cronin effect: significant enhancement of baryon relative to meson yields for $p_T \sim$ few GeV/c has been measured in fixed target p+A measurements⁴² and may be attributable to initial state multiple scattering, though this measurement must be repeated at RHIC energies for quantitative comparison. More exotic mechanisms such as baryon production via gluonic junctions⁴³ have also been discussed in this context.

The ratios in fig. 14 are measured to $p_T \sim 4$ GeV/c. It is important to establish whether the anomalous baryon enhancement for central collisions extends to higher p_T or whether the conventional jet fragmentation ratio is re-established. As a step in that direction, fig. 15 shows the ratio of π^0 to all charged hadrons for $p_T < 9$ GeV/c, for minimum bias Au+Au events. Even for minimum bias the ratio is suppressed relative to the conventional expectation of 0.7-0.8. This presents an important puzzle, but more detailed centrality dependence and explicit measurement of the baryon and meson fractions would help to elucidate this phenomenon.

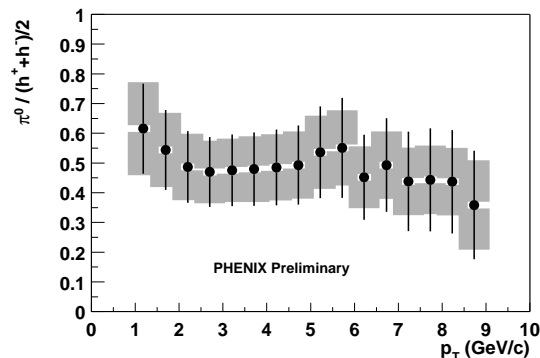


Fig. 15. Ratio of π^0 to total charged hadron yield vs. p_T from minimum bias Au+Au collisions at 200 GeV.³⁰

4.5 High p_T : Discussion

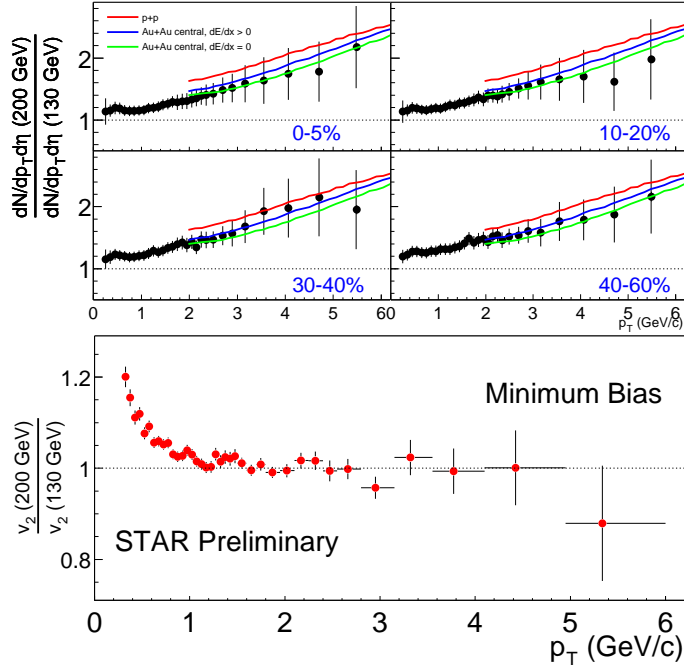
The foregoing sections reveal the following facts about high p_T hadron production in Au+Au collisions at RHIC energies:

- Inclusive hadron production is suppressed in central collisions by a factor 4-5, with no strong p_T dependence within $5 < p_T < 12$ GeV/c.
- For non-central collisions, finite azimuthal correlations of leading hadrons with the reaction plane persist to $p_T \sim 10$ GeV/c.
- Near-angle two particle correlations show clear jet-like correlations for $p_T > 4$ GeV/c.

- Back-to-back two particle correlations show a striking suppression in central collisions.
- The baryon/meson ratio for $p_T < 4$ GeV/c is strongly enhanced in central collisions, whereas it is consistent with jet fragmentation in vacuum for peripheral collisions.

All but the last of these phenomena suggest a picture in which the system generated in nuclear collisions at RHIC is largely opaque to high energy partons and only those jets produced on the periphery of the reaction zone and heading outwards survive and are observed. This scenario naturally generates the suppression of the inclusive spectra and the space-momentum correlation that produces $v_2(p_T)$, as well as the strong suppression of back-to-back pairs.

Additional support for this picture comes from Fig. 16, which shows the \sqrt{s} dependence of the inclusive yields and $v_2(p_T)$ between $\sqrt{s_{NN}}=130$ and 200 GeV. The lines in the upper figure show the pQCD expectation of the growth of inclusive cross section with \sqrt{s} for p+p and Au+Au (with and without energy loss). The inclusive rates grow by a factor 2 at $p_T \sim 6$ GeV/c, consistent with expectations from pQCD, Fig. 16. \sqrt{s} dependence of inclusive yields and whereas $v_2(p_T)$ is independent of $\sqrt{s_{NN}}$ at the 5% level



for $p_T > 2$ GeV/c. The inclusive rates grow but the anisotropy does not change, suggesting that the origin of $v_2(p_T)$ is geometric, not dynamic.

However, this picture as presented is only qualitative, and it remains to be shown whether a surface emission model can simultaneously describe the inclusive suppression, $v_2(p_T)$, and the suppression of back-to-back pairs. The anomalous baryon/meson

ratio presents a puzzle and does not seem to fit into this picture. That effect may be due to conventional mechanisms such as transverse radial flow or initial state multiple scattering, or more exotic physics such as baryon production via gluonic junctions.⁴³ Further analysis of existing data and measurements of d+Au collisions at RHIC are needed to clarify these issues.

Finally, it is necessary to establish what, precisely, is interacting with the medium and being absorbed: partons or hadrons? Simple estimates of hadron formation time give $t_f \sim (E/m)r$ for a hadron of radius r ,⁴⁴ so that a pion with $p_T \sim 5$ GeV/c is formed well outside of the hot and dense medium. Alternatively, string interactions in matter prior to fragmentation lead to suppression the leading particle yields and a much shorter apparent formation time for high p_T hadrons.⁴⁵

5 Summary and Outlook

RHIC has had two successful data-taking periods. It has met its design luminosity goal for Au+Au, and has operated as the world's first polarized proton collider. Upcoming runs in 2003 will study asymmetric (d+Au) collisions for the first time in a collider, together with an extended polarized proton run. A long Au+Au run at top energy will occur in 2004, possibly with an energy scan at lower integrated luminosity.

An extensive array of measurements in the soft physics sector indicate the production of an equilibrated system at high temperature and pressure which blows apart rapidly. In the high p_T sector, striking signals have been observed that suggest strong partonic energy loss resulting from a system at high energy density at early time, though there remain important puzzles and open questions.

I have not discussed the study of heavy quark production, which is in its infancy at RHIC. Charmonium suppression, a promising signature of deconfinement,⁸ has been observed in fixed-target nuclear collisions at the SPS.⁴⁶ PHENIX has measured the inclusive electron spectrum, due primarily to charm,⁴⁷ and recently reported the first measurement of J/ψ at RHIC.⁴⁸ This physics will be a main focus of future runs.

References

- [1] J. C. Collins and M. J. Perry, Phys. Rev. Lett. **34**, 1353 (1975).
- [2] K. Rajagopal and F. Wilczek, hep-ph/0011333.

- [3] K. Kanaya, hep-ph/0209116.
- [4] F. Karsch, Nucl. Phys. **A698**, 199c (2002).
- [5] Z. Fodor, hep-lat/0209191.
- [6] D. Boyanovsky, hep-ph/0102120.
- [7] N. K. Glendenning and F. Weber, astro-ph/0003426.
- [8] J. W. Harris and B. Müller, Annu. Rev. Nucl. Part. Sci. **B46**, 71 (1966).
- [9] T. Roser, Nucl. Phys. **A698**, 23c (2002).
- [10] BRAHMS (www4.rcf.bnl.gov/brahms/WWW/brahms.html); PHOBOS (phobos-srv.chm.bnl.gov); PHENIX (www.phenix.bnl.gov); STAR (www.star.bnl.gov).
- [11] Proceedings of Quark Matter 2001, Stony Brook, N.Y., Jan. 15-21, 2001, Nucl. Phys. **A698** (2002).
- [12] Quark Matter 2002, Nantes, France, July 11-18 2002 (<http://alice-france.in2p3.fr/qm2002/>).
- [13] C. Adler *et al.*, Nucl. Instr. Meth. **A461**, 337 (2001)
- [14] K. Adcox *et al.* (PHENIX Collaboration), Phys. Rev. Lett. **86**, 3500 (2001).
- [15] D. E. Kharzeev and J. Raufeisen, nucl-th/0206073.
- [16] B. B. Back *et al.* (PHOBOS Collaboration), nucl-ex/0210015.
- [17] Studies of inclusive reactions use the kinematic variables transverse momentum p_T , rapidity $y = \frac{1}{2} \log\left(\frac{E+p_z}{E-p_z}\right)$, and its relativistic limit pseudorapidity $\eta = -\log(\tan(\theta/2))$.
- [18] T. Ullrich, nucl-ex/0211004.
- [19] J. D. Bjorken, Phys. Rev. **D27**, 140 (1983).
- [20] K. Adcox *et al.* (PHENIX Collaboration), Phys. Rev. Lett. **87**, 052301 (2001)
- [21] B. Back *et al.* (PHOBOS Collaboration), Phys. Rev. **C65**, 061901R (2002).
- [22] P. Steinberg *et al.* (PHOBOS Collaboration), nucl-ex/0211002.
- [23] P. Braun-Munzinger, D. Magestro, K. Redlich and J. Stachel, Phys. Lett. **B518**, 41 (2001).
- [24] J. D. Bjorken, FERMILAB-Pub-82/59-THY.
- [25] M. Gyulassy and M. Plümer, Phys. Lett. **B243**, 432 (1990); R. Baier *et al.*, Phys. Lett. **B345**, 277 (1995).

- [26] R. Baier, D. Schiff and B. G. Zakharov, *Annu. Rev. Nucl. Part. Sci.* **B50**, 37 (2000).
- [27] X. N. Wang and M. Gyulassy, *Phys. Rev. Lett.* **68**, 1480 (1992); X. N. Wang, *Phys. Rev.* **C58**, 2321 (1998).
- [28] E. Wang and X. N. Wang, *Phys. Rev. Lett.* **89**, 162301 (2002); F. Arleo, *Phys. Lett.* **B532**, 231 (2002).
- [29] K. Adcox *et al.* (PHENIX Collaboration), *Phys. Rev. Lett.* **88**, 022301 (2002); C. Adler *et al.* (STAR Collaboration), *Phys. Rev. Lett.* **89**, 202301 (2002).
- [30] S. Mioduszewski *et al.* (PHENIX Collaboration), nucl-ex/0210021.
- [31] J. Klay *et al.* (STAR Collaboration), nucl-ex/0210026.
- [32] I. Vitev and M. Gyulassy, hep-ph/0209161.
- [33] H. Sorge, *Phys. Rev. Lett.* **82**, 2048 (1999); P. Kolb, J. Sollfrank and U. Heinz, *Phys. Rev.* **C62**, 054909 (2000).
- [34] C. Adler *et al.* (STAR Collaboration), *Phys. Rev. Lett.* **86**, 402 (2001); *Phys. Rev. Lett.* **87**, 182301 (2001).
- [35] M. Gyulassy, I. Vitev and X. N. Wang, *Phys. Rev. Lett.* **86**, 2537 (2001).
- [36] Use of the term “elliptic flow” to describe the azimuthal correlation of jet products with the reaction plane orientation is unfortunate but firmly entrenched in the literature.
- [37] E. V. Shuryak, nucl-th/0112042.
- [38] C. Adler *et al.* (STAR Collaboration), nucl-ex/0206006.
- [39] K. Filimonov *et al.* (STAR Collaboration), nucl-ex/0210027.
- [40] C. Adler *et al.* (STAR Collaboration), nucl-ex/0210033.
- [41] P. Abreu *et al.* (DELPHI Collaboration), *Phys. Lett.* **B407**, 174 (1997).
- [42] P. B. Straub *et al.*, *Phys. Rev. Lett.* **452**, 68 (1992).
- [43] I. Vitev and M. Gyulassy, *Phys. Rev.* **C65**, 041902 (2002).
- [44] Y. L. Dokshitzer, V. A. Khoze, A. H. Mueller and S. I Troyan, “Basics of Perturbative QCD”, Editions Frontières, Gif-Sur-Yvette, 1991.
- [45] B. Z. Kopeliovich, *Phys. Lett.* **B243**, 141 (1990).
- [46] M. C. Abreu *et al.* (NA50 Collaboration), *Nucl. Phys.* **A698**, 127c (2002).

- [47] K. Adcox *et al.* (PHENIX Collaboration), Phys. Rev. Lett. **88**, 192302 (2002).
- [48] J. Nagle *et al.* (PHENIX Collaboration), nucl-ex/0209015.